J. Biomed. Eng. Res.
Vol.26, No.4, 215-221, 2005

# Development of Prototype Multi-channel Digital EIT System with Radially Symmetric Architecture

Tong In Oh[1], Sang Min Baek[1], Jae Sang Lee[1], Eung Je Woo[1], Chun jae Park[2]

[1]Department of Biomedical Engineering, Kyung Hee University
[2]Impedance Imaging Research Center, Kyung Hee University
*(Received April 22, 2005. Accepted July 28, 2005)*

**Abstract:** We describe the development of a prototype multi-channel electrical impedance tomography (EIT) system. The EIT system can be equipped with either a single-ended current source or a balanced current source. Each current source can inject current between any chosen pair of electrodes. In order to reduce the data acquisition time, we implemented multiple digital voltmeters simultaneously acquiring and demodulating voltage signals. Each voltmeter measures a differential voltage between a fixed pair of adjacent electrodes. All voltmeters are configured in a radially symmetric architecture to optimize the routing of wires and minimize cross-talks. To maximize the signal-to-noise ratio, we implemented techniques such as digital waveform generation, Howland current pump circuit with a generalized impedance converter, digital phase-sensitive demodulation, tri-axial cables with both grounded and driven shields, and others. The performance of the EIT system was evaluated in terms of common-mode rejection ratio, signal-to-noise ratio, and reciprocity error. Future design of a more innovative EIT system including battery operation, miniaturization, and wireless techniques is suggested.

**Key words:** EIT, Radially symmetric architecture, Current source, Voltmeter

## INTRODUCTION

When we inject current into an electrically conducting subject such as the human body through a pair of surface electrodes, the internal current pathway is determined by the conductivity and permittivity distribution and the geometry of the subject. In this paper, we assume a relatively low operating frequency and neglect the effect of the permittivity. Any local change of the conductivity distribution results in a change of the internal current pathway whose effect is conveyed to boundary voltages.

Electrical impedance tomography (EIT) is to visualize images of a conductivity distribution inside the human body [1-3]. In EIT, measured boundary voltages due to multiple injection currents are used to reconstruct an image of the conductivity distribution. However, these boundary voltages are insensitive to a local change of the conductivity distribution and the relation between them is highly nonlinear.

This work was supported by the grant R11-2002-103 from the Korea Science and Engineering Foundation (KOSEF).
**Corresponding Author:** Eung Je Woo
Department of Biomedical Engineering College of Electronics and Informations Kyung Hee University, 1 Seochun, Kiheung, Yongin, Kyungki, 449-701, Korea
Tel. 031-201-2538 Fax. 031-201-2378
E-mail. ejwoo@khu.ac.kr

EIT, therefore, suffers from the ill-posed characteristics of the corresponding inverse problem. This requires a very accurate measurement technique and EIT is still in its early stage of technology development especially in terms of the required measurement system.

Any EIT system for clinical uses must satisfy the following requirements. First, the injection current must be accurate and stable in terms of its amplitude, frequency, and phase against a resistive and capacitive load of about 1KΩ at an operating frequency of 10KHz or higher. Second, the voltmeter to measure the induced boundary voltage must be accurate with an overall measurement error of about 0.1%. It should be able to measure both the magnitude and phase of the voltage signal. Third, the data acquisition must be done in real-time to be able to show changes in conductivity subject to any fast physiological events. This is to preserve the advantage of EIT in terms of its temporal resolution over other imaging modalities with relatively higher spatial resolution and low temporal resolution. Considering the numerous image reconstruction algorithms already developed [3], the most needed job in the development of a clinical EIT system is the hardware technology development providing accurate boundary current-voltage measurements. The primary goal of the paper is to develop new EIT hardware techniques for the reduction

of measurement errors.

There exist several EIT systems already developed with different design concepts and technical details in their implementations. We may classify recent EIT systems into two types. The first can be characterized as having one active current source. In this case, we inject current between a chosen pair of electrodes. The second type uses multiple current sources. Here, we inject a pattern of current through multiple electrodes using multiple active current sources. The sum of currents from all active current sources must be zero and there should be no phase difference among them. In most current EIT systems belonging to both types, voltages from all or selected electrodes are simultaneously measured using multiple voltmeters. Typical examples of the first and second type are Mk3.5 from Sheffield [4] and ACT-3 from RPI [5], respectively.

Even though the second type may have some advantage in terms of the distinguishability [6], we decided to adopt the first type considering the factors described below: (a) complexity of the system, (b) technology currently available for us, and (c) future direction of EIT system development including miniaturization and wireless interconnection. Other functional limitations in trans-impedance measurements summarized by Seagar and Brown [7] and Brown and Seagar [8] have been also considered.

This paper describes the second generation of our EIT system with multiple voltmeters and a single current source. The first generation was described in [9]. After explaining the new radially symmetric architecture, we will describe each part of the system including current source, multi-channel digital voltmeters, interconnections, RF data linkage, and software. The performance of the developed EIT system was evaluated using a resistor and saline phantom in terms of stability, common-mode rejection ratio (CMRR), signal-to-noise ratio (SNR), and reciprocity error (RE). EIT images from saline phantoms by using the developed EIT system are also presented.

# METHODS

## System Architecture

The developed EIT system shown in Fig. 1 consists of the following parts: (a) a current source, (b) multiple voltmeters, (c) a main controller with wireless RF data link, and (d) a PC with control and data acquisition software. We tried to minimize the amount of analog circuits as much as possible throughout the system. This was realized by using field programmable gate arrays (FPGA). The main controller (TMS320LF2407A, Texas Instruments, USA) controls the current source and all voltmeters. It also provides a 40MHz clock signal to the rest of the system for the synchronization of the current source and all voltmeters.

The unique feature of the system is its radially symmetric architecture. Data links between the main controller and the rest of the system including current source and voltmeters are one-to-one half-duplex high-speed serial data communication channels in a star topology. A similar approach can be found in the design of a high-speed EIT system for imaging the breast [10].

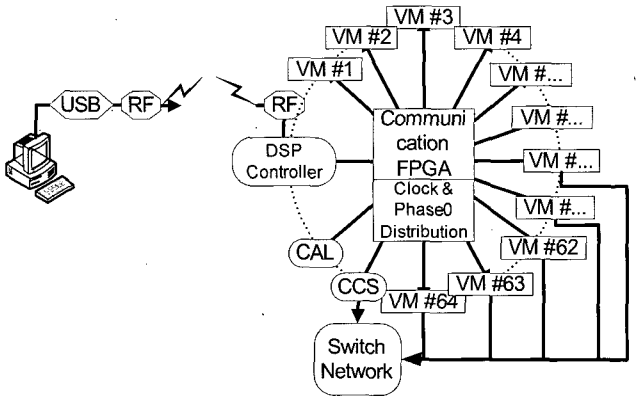


**Fig. 1.** Configuration of the developed EIT system.

## Constant Current Source

The performance of the constant current source is one of the major limiting factors determining the accuracy of an EIT system. We designed and implemented the constant current source including the FPGA-based waveform generator, voltage-to-current converter, and automatic calibration circuit.

Nebuya *et al.* studied the accuracy in tetra-polar trans-impedance measurements [11]. They suggested optical isolations of both current source and voltmeter to minimize the undesirable effects of stray capacitances between wires and also between current source and voltmeter. Fig. 2(a) shows the block diagram of an isolated current source used in this paper. This single-ended constant current source is optically isolated from the rest of the circuits including all voltmeters to minimize cross-talks due to stray capacitances. For the isolation of the current source, we used a digital isolator (AduM1100, Analog Devices, USA) with 100Mbps throughput. The time delay in the trigger pulse for sinusoidal wave generation before and after the digital isolator was measured as 15ns using a digital oscilloscope with 2.5GHz analog bandwidth, 10GHz sampling rate, and 1ps time resolution (TDS7254, Tektronix, USA).

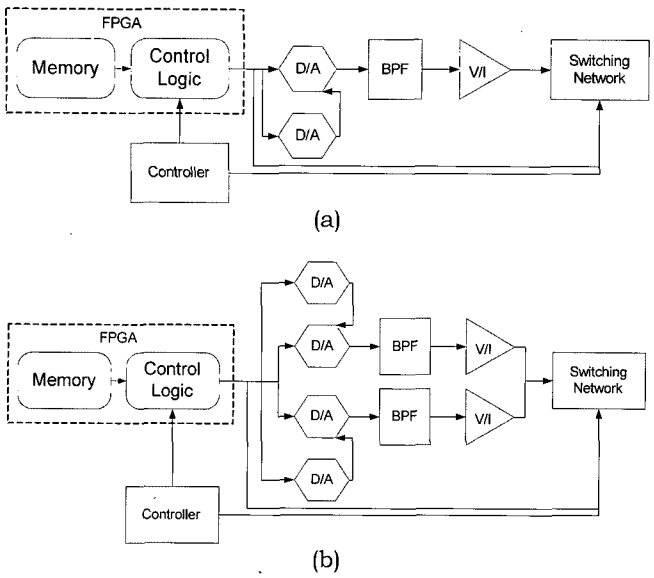


**Fig. 2.** Block diagram of constant current sources: (a) isolated single-ended current source and (b) non-isolated balanced current source.

We also implemented a non-isolated balanced current source shown in Fig. 2(b). In both current sources, we generated a sinusoidal voltage signal with variable amplitude using an FPGA (Acex, Altera, USA) and a 16-bit DAC (AD768, Analog Devices, USA). The voltage signal is converted to current using the improved Howland current pump circuit [12].

In order to maximize the output impedance of the current sources, we used two digital potentiometers (DS1267, Dallas Semiconductors, USA). One is used to balance the values of five resistors in the improved Howland current pump circuit and the other is used in the generalized impedance converter (GIC) to cancel out the stray capacitance at the output of the current source [12,13]. We designed the current sources to have the output impedance of 64M□. This is to keep the accuracy of 16-bit assuming the maximal load impedance of 1K□ that is approximately $64{,}000/2^{16}$K□. Automatic calibrations of the current sources were implemented following the method described by Cook *et al.* [5]. The output of each current source is connected to a chosen pair of electrodes through a switching network using T-bar switches (MAX4545, Maxim, USA) with a negligible amount of cross-talks.

## Multi-channel Digital Voltmeters

We designed and implemented digital voltmeters for the EIT system based on the digital phase-sensitive demodulation technique. Each voltmeter consists of the following parts: (a) shield drive circuit using an operational amplifier (AD8039, Analog Devices, USA) for the tri-axial cable (SML50, Habia Cable, Sweden), (b) differential amplifier (AD8130, Analog Devices, USA) with gain of one, (c) 0° phase delay passive band-pass filter, (d) voltage amplifiers with variable gain using operational amplifiers (AD8039, Analog Devices, USA), (e) 12-bit ADC (AD9235, Analog Devices, USA) at 10MHz sampling frequency with the non-uniform sampling technique [5,9], and (f) FPGA (Acex, Altera, USA). The FPGA includes a spike noise-rejection filter, an automatic gain controller, two digital phase-sensitive demodulators, and signal averaging. The FPGA controls the gain of the analog voltage amplifier using a digital potentiometer (DS1267, Dallas Semiconductor, USA). Fig. 3 shows the block diagram of the analog part of each voltmeter. Details other than the analog part are described in [9]. We designed the voltmeter to have the SNR of 104dB by appropriately choosing the number of required data samples for signal averaging [5,9].

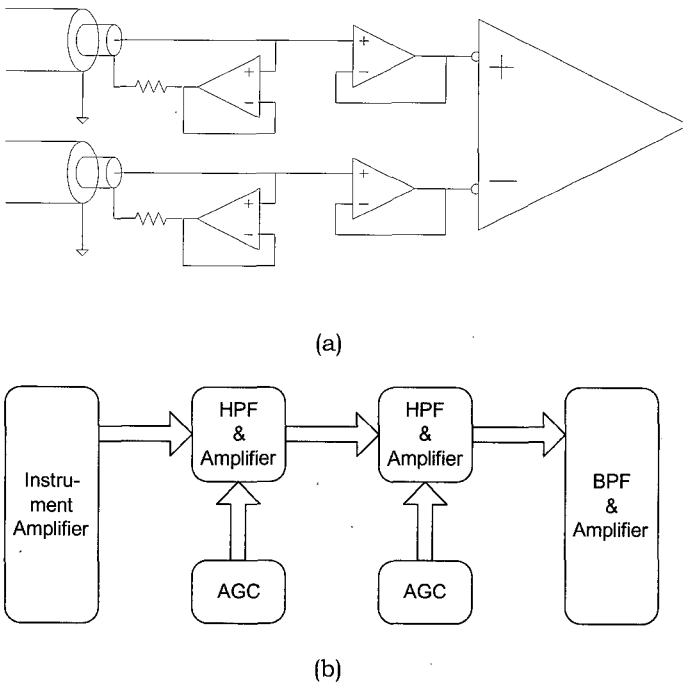


**Fig. 3.** Block diagram of the analog part of the voltmeter: (a) shield drive and tri-axial cable connection and (b) filter and gain stages.

## Serial Interconnections

The main controller should collect in-phase and quadrature components of the measured voltage signals from all voltmeters to transmit the data to the

PC. Each FPGA in the voltmeter or current source communicates with the main controller through a half-duplex high-speed synchronous serial communication network. In the digital backplane board, two master communication FPGAs arbitrate data transmission between the FPGA in each voltmeter or current source and the main controller. Fig. 5 shows the block diagram of the communication FPGA for the interconnections. This kind of serial interconnections significantly reduces the digital noise in voltmeters and current source.

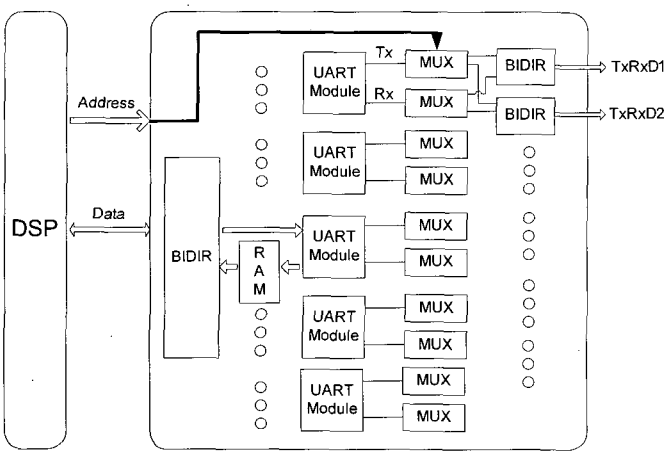


**Fig. 4.** Block diagram of the communication FPGA for serial interconnections.

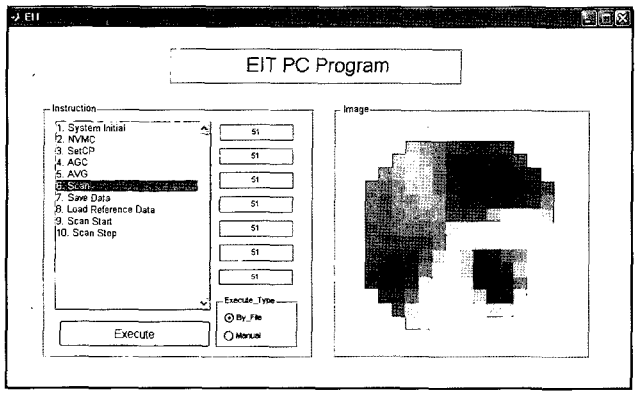


**Fig. 5.** EIT PC software.

### RF Data Linkage to a PC and Software

For the data exchanges with a PC, the main controller is interfaced to a 2.4GHz RF serial link module (RFW112, RFWaves, Israel) at 1Mbps data rate. In the PC, we developed a custom designed USB interface card using an USB controller (C8051F320, Silicon Lab., USA). The USB card also includes the same 2.4GHz RF serial link module. The control and data acquisition software in the PC was developed using Matlab (Mathworks, USA). Fig. 5 shows the developed EIT software using Matlab. The developed software includes data communication with the main controller of the EIT system, dynamic image reconstructions, and image display.

## RESULTS

### Basic Performance Test

Fig. 6 shows the developed EIT system with 64 voltmeters. The number of voltmeters can be reduced to 32, 16, or 8. The output impedance of the current source was found to be greater than 1GΩ at low frequency but it was reduced down to 3.6MΩ at the operating frequency of 50KHz. This suggests further improvements in canceling the stray capacitances at the output of the current source.

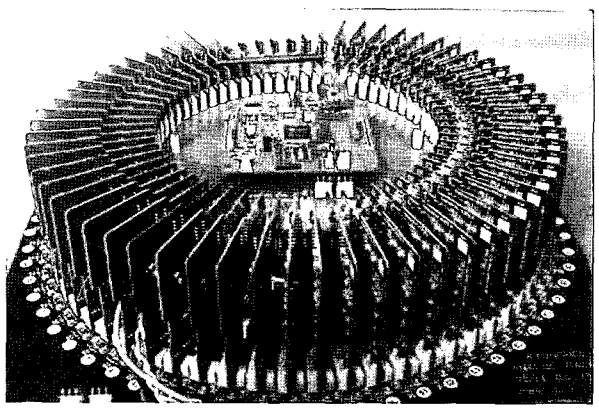

**Fig. 6.** Developed 64-channel EIT system. The number of channels can be reduced to 32,16, or 8.

In both of the developed constant current sources, the total harmonic distortion (THD) was 0.03% and the amplitude stability error was 0.2445% over one hour. The stability error over a short time period of voltage measurements was negligibly small. At low frequency, the optical isolation of the single-ended current source was effective in reducing stray capacitances. However, at the operating frequency of 50KHz, the effect of the optical isolation was significantly reduced. This result suggests that the isolated single-ended current source

is desirable at low frequency (below 100Hz) and the balanced current source is recommended at higher frequency.

The CMRR of the voltmeter was measured as about 100dB. The voltmeters were experimentally tested to have the SNR of about 70 to 85dB depending on channels. The reciprocity errors (REs) were less than 1% with the mean value of 0.5%.

## Resistor Phantom Test

We used a resistor phantom to simultaneously test all of the voltmeters in the EIT system. The resistor phantom is a simple electric circuit with connected resistors of known resistance values. Injecting currents between pairs of adjacent resistors, we measured voltages between other pairs of adjacent resistors in the resistor phantom. Comparing the measured data from the resistor phantom with the numerical simulation (i.e., circuit analysis) result, we found that the measured data need to be calibrated to compensate the difference shown in Fig. 7. With calibrations of all voltmeters using known resistive loads, we could compensate channel-dependent magnitude and phase errors.

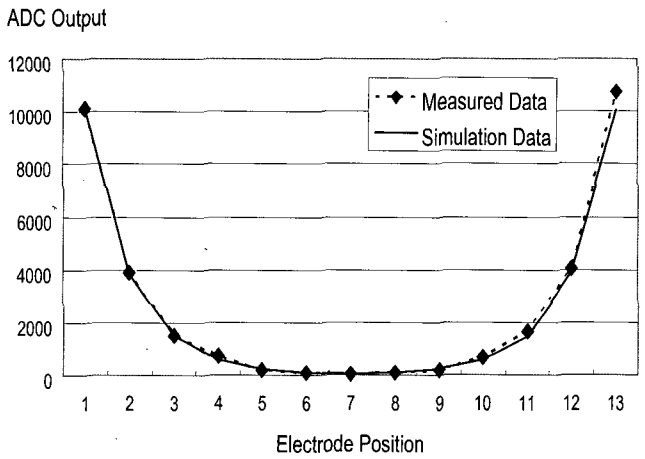


**Fig. 7.** Measured magnitude data before calibrations and simulation (i.e., circuit analysis) data from a resistor phantom with connected resistors of known resistance values. Calibration was performed to match the two data sets.

## Saline Phantom Test

Fig. 8(a) shows a cylindrical saline phantom with 200mm diameter and 100mm height. It was filled with a saline of 0.44S/m conductivity. A cylindrical anomaly made of acrylic plastic with 30mm diameter was placed inside the phantom near the electrode position between 10 and 11 in Fig. 8(b). Comparing the measured voltage data with and without the anomaly, we found that they show a clear difference as shown in Fig. 8(b).

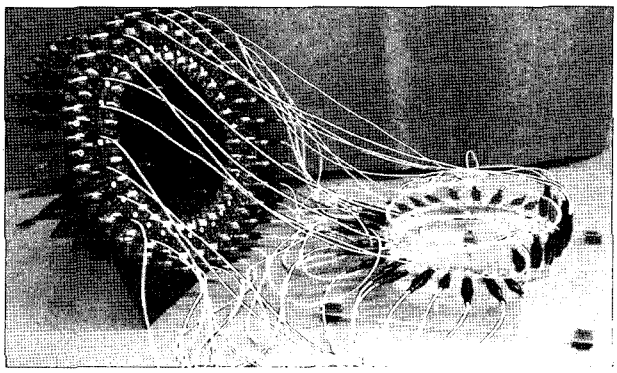

(a)

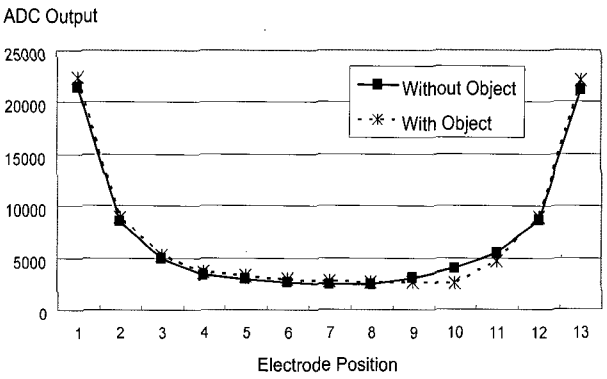


(b)

**Fig. 8.** Saline phantom experiments: (a) saline phantom and (b) measured magnitude data with and without an object located near the electrode position between 10 and 11.

## EIT Images

Fig. 9(a) shows the same saline phantom including a conductor with 30mm diameter and an insulator with the same size. The positions of the objects are shown in Fig. 9(a). We measured a full set of boundary voltages before and after we placed the objects and reconstructed the conductivity difference image shown in Fig. 9(b). Here, the blue and red colours indicate decrease and increase in conductivity, respectively. Fig. 10 shows another saline phantom with an agar object and its conductivity difference image. In Fig. 10, the background solution has a conductivity of 0.067S/m and the circular agar object with 30mm diameter has a conductivity of 0.9S/m.

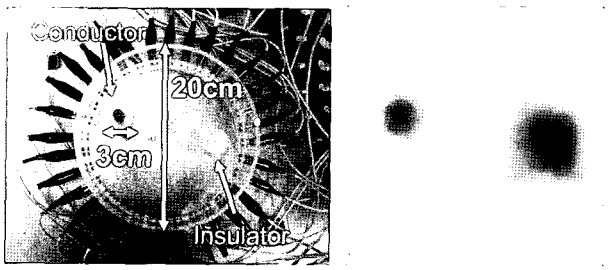


(a) (b)

**Fig. 9. (a)** *Saline phantom with a conductor and an insulator.* (b) Conductivity difference image of the phantom in (a) before and after placing the objects.

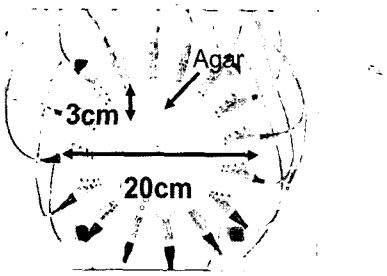


(a) (b)

**Fig. 10.** (a) Saline phantom with an agar object. (b) Conductivity difference image of the phantom in (a) before and after placing the agar object.

## DISCUSSION

The EIT system described in this paper is the second generation system developed at the Impedance Imaging Research Center (IIRC) in Korea. Solving most technical problems raised from the first generation system [9], the current EIT system outperforms the previous one in terms of all performance indices. Major features of the system are as follows. These new features enabled the EIT system to enhance its performance beyond other EIT systems of the same type.

(a) Radially symmetric architecture with star topology and serial communication link
(b) FPGA-based design for digital implementation of most functions
(c) Automatic gain control and spike noise rejection in each voltmeter

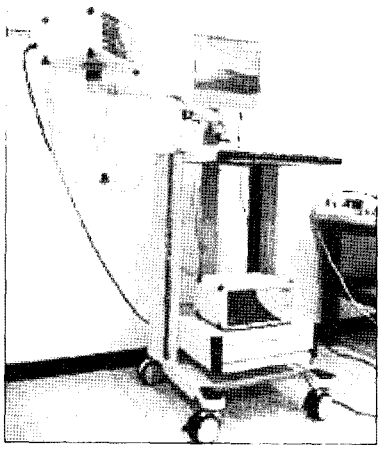

**Fig. 11.** Mk3.5 (Maltron, UK): a commercial EIT system with eight channels.

Fig. 11 shows a picture of a commercial eight-channel EIT system (Mk3.5, Maltron, UK) installed in our laboratory. It is the only commercial EIT system available for researchers [4]. Its voltmeter SNRs were measured as 58 to 73dB depending on channels and reciprocity error (RE) was evaluated as 1.4%. Since Mk3.5 is an eight-channel multi-frequency system, we measured these parameters at the fixed operating frequency of 50KHz. Comparing these values with those of our EIT system described in previous section, we found that our system outperforms Mk3.5 in terms of SNR and RE mainly due to its radially symmetric architecture.

In EIT, we do not aim for conductivity imaging with a high spatial resolution. We only try to visualize changes in conductivity distribution with a low spatial resolution and high temporal resolution. This is due to the fundamental limitations related with the ill-posedness of the corresponding inverse problem. Therefore, we plan to look for application areas of EIT technique where its high temporal resolution and portability are of significant merits [1-3]. Describing the technical details of the system in this paper, we will perform numerous experimental studies for various applications areas of EIT as described in [3]. For a high-resolution conductivity imaging, we are developing a new technique called Magnetic Resonance Electrical Impedance Tomography (MREIT) [14,15].

Future improvements in the EIT hardware development should include the followings.

(a) Multi-frequency mode for spectroscopic impedance imaging
(b) Higher-speed RF data link between the EIT system and a PC
(c) Wearable human interface

(d) Miniaturization of circuits for a wireless smart electrode
(e) Sequencing and synchronization among wireless smart electrodes
(f) Wireless multi-channel data communication among smart electrodes
(g) Electrode position sensing
(h) Power supply for the wireless smart electrode

The next version will include the solutions for (a) to (c) in the above list. The items (d) to (h) present quite a lot of technical challenges. Significant amount of serious research efforts are needed for these items and we plan to keep accumulating experiences in EIT hardware development for those quite challenging tasks.

## CONCLUSION

The developed system is the first EIT system with the radially symmetric architecture providing superior performance to the existing systems with one active current source and multiple voltmeters. We found that multiple voltmeters simultaneously acquiring and demodulating voltage signals are essential in order to reduce the data acquisition time for fast imaging. The wireless data communication between the EIT system and a PC is desirable in terms of noise and electrical safety.

As a short term research goal, we should apply the developed EIT system to numerous potential application areas in biomedicine and non-destructive testing. We plan to keep improving the performance of the system and accumulate the skills in EIT hardware development so that we can miniaturize the circuits for a new EIT system with wireless smart electrodes.

## REFERENCES


[1] J. G. Webster, ed., Electrical Impedance Tomography, Adam Hilger, Bristol, UK, 1990.

[2] K. Boone, D. Barber, and B. H. Brown, *"Imaging with electricity: report of the European concerted action on impedance tomography"*, J. Med. Eng. Tech., Vol. 21, pp. 201-232, 1997.

[3] D. Holder, ed., Electrical Impedance Tomography: Methods, History and Applications, IOP Publishing, London, UK, 2005.

[4] A. J. Wilson, P. Milnes, A. R. Waterworth, R. H. Smallwood, and B. H. Brown, *"Mk3.5: a modular, multi-frequency successor to the Mk3a EIS/EIT system"*, Physiol. Meas., Vol. 22, pp. 49-54, 2001.

[5] R. D. Cook, G. J. Saulnier, D. G. Gisser, J. G. Goble, J. C. Newell, and D. Isaacson, *"ACT3: a high-speed, high-precision electrical impedance tomography"*, IEEE Trans. Biomed. Eng., Vol. 41, pp. 713-722, 1994.

[6] D. Isaacson, *"Distinguishability of conductivities by electric current computed tomography"* , IEEE Trans. Med. Imag., Vol. 5, pp. 91-95, 1986.

[7] A. D. Seagar and B. H. Brown, *"Limitations in hardware design in impedance imaging"* , Clin. Phys. Physiol. Meas., Vol. 8 Suppl. A, pp. 85-90, 1987.

[8] B. H. Brown and A. D. Seagar, *"The Sheffield data collection system"* , Clin. Phys. Physiol. Meas., Vol. 8 Suppl. A, pp. 91-97, 1987.

[9] T. I. Oh, S. M. Baek, J. S. Lee, and E. J. Woo, *"Design and implementation of digital electrical impedance tomography system"* , J. Biomed. Eng. Res., Vol. 25, No. 4, pp. 269-275, 2004.

[10] R. Halter, A. Hartov, and K. D. Paulsen, *"Design and implementation of a high frequency electrical impedance tomography system"* , Physiol. Meas., Vol. 25, pp. 379-390, 2004.

[11] S. Nebuya, M. Noshiro, B. H. Brown, R. H. Smallwood, and P. Milnes, *"Accuracy of an optically isolated tetra-polar impedance measurement system"* , Med. Biol. Eng. Comput., Vol. 40, pp. 647-649, 2002.

[12] S. Franco, Design with Operational Amplifiers and Analog Integrated Circuits, 3rd. ed., McGraw-Hill, NY, USA, 2002.

[13] A. S. Ross, G. J. Saulnier, J. C. Newell, and D. Isaacson, *"Current source design for electrical impedance tomography"* , Physiol. Meas., Vol. 24, pp. 509-516, 2003.

[14] E. J. Woo, J. K. Seo, and S. Y. Lee, *"Magnetic resonance electrical impedance tomography"* , in D. Holder, ed., Electrical Impedance Tomography: Methods, History and Applications, IOP Publishing, London, UK, 2005.

[15] S. H. Oh, B. I. Lee, E. J. Woo, S. Y. Lee, T. S. Kim, O. Kwon, and J. K. Seo, *"Electrical conductivity images of biological tissue phantoms in MREIT"*, Physiol. Meas., Vol. 26, pp. S279-S288, 2005.